



Fictitious magnetic-field gradients in optical microtraps as an experimental tool for interrogating and manipulating cold atoms

B. Albrecht, Y. Meng, C. Clausen, A. Dureau, P. Schneeweiss,* and A. Rauschenbeutel†

Vienna Center for Quantum Science and Technology, TU Wien–Atominstytut, Stadionallee 2, 1020 Vienna, Austria

(Received 9 September 2016; published 30 December 2016)

Optical microtraps provide a strong spatial confinement for laser-cooled atoms. They can, e.g., be realized with strongly focused trapping light beams or the optical near fields of nanoscale waveguides and photonic nanostructures. Atoms in such traps often experience strongly spatially varying ac Stark shifts which are proportional to the magnetic quantum number of the respective energy level. These inhomogeneous fictitious magnetic fields can cause a displacement of the trapping potential that depends on the Zeeman state. Hitherto, this effect was mainly perceived as detrimental in optical microtraps. However, it also provides a means to probe and to manipulate the motional state of the atoms in the trap by driving transitions between Zeeman states. Furthermore, by applying additional real or fictitious magnetic fields, the state dependence of the trapping potential can be controlled. Here, using laser-cooled atoms that are confined in a nanofiber-based optical dipole trap, we employ this control in order to tune the microwave coupling of motional quantum states. We record corresponding microwave spectra which allow us to infer the trap parameters as well as the temperature of the atoms. Finally, we reduce the mean number of motional quanta in one spatial dimension to $\langle n \rangle = 0.3(1)$ by microwave sideband cooling. Our work shows that the inherent fictitious magnetic fields in optical microtraps expand the experimental toolbox for interrogating and manipulating cold atoms.

DOI: [10.1103/PhysRevA.94.061401](https://doi.org/10.1103/PhysRevA.94.061401)

Optical dipole forces are a ubiquitous tool for trapping and manipulating ultracold atoms. Notable achievements with optical dipole traps include the investigation of quantum-degenerate gases [1,2], quantum simulation of many-body systems in optical lattices [3], long-lived quantum memories for light [4], and optical frequency standards and precision spectroscopy [5]. Optical microtraps confine a single or a few atoms to a small volume. They can, for example, be formed in the focus of a lens [6,7] and have recently been employed, e.g., to study Rydberg interactions [8,9] or the collisional entangling dynamics between two atoms [10]. Microtraps have also been created in the near field of optical nanofibers. They offer a strong transverse confinement of the guided light over their full length and thereby enable a homogeneous and efficient coupling to ensembles of trapped atoms [11,12]. In addition, nanostructuring dielectric waveguides allows one to engineer their dispersion, e.g., to drastically enhance the coupling between the atoms and the guided mode [13]. Nanoscale photonic waveguides thereby open the route towards ultrastrong optical nonlinearities [14] and the study of new effects such as atom-photon bound states [15].

For atoms in optical traps, elliptical polarization components of the trapping light fields in general give rise to Zeeman state-dependent energy shifts that are equivalent to the effect of a fictitious magnetic field [16]. A spatially varying intensity or ellipticity of the light then leads to a gradient of this fictitious magnetic field which is at the heart of sub-Doppler laser cooling [17] and has been employed to, e.g., demonstrate an optical analog of the Stern-Gerlach effect [18]. The intentional introduction of such fictitious magnetic-field gradients into optical lattices enabled the demonstration of Raman sideband cooling [19–21], coherent spin-dependent transport [22],

quantum walks [23], selective addressing of qubits [24], and microwave sideband cooling in state-dependent potentials [25,26]. In optical microtraps, a spatially varying elliptical polarization occurs naturally [27]: According to Gauss' law the local ellipticity depends on the divergence of the transverse field components [28,29]. Remarkably, when the transverse field components vary significantly on the wavelength scale, the local polarization can be almost perfectly circular even when the transverse field is linearly polarized. The strongly inhomogeneous fictitious magnetic field that occurs in such situations is usually considered to be detrimental: It gives rise to a Zeeman state-dependent displacement of the trap minimum which may lead to dephasing, reduced fidelities in optical pumping, and heating [30]. Therefore, so far, the effects of confinement-induced fictitious magnetic fields have typically been suppressed in experiments [30–32].

Here, we take advantage of confinement-induced fictitious magnetic fields in order to couple the motional state of atoms in a nanofiber-based optical dipole trap with their internal hyperfine states via microwave transitions. We record corresponding microwave spectra which allow us to infer the trap parameters as well as the temperature of the atoms. Furthermore, by applying additional homogeneous real magnetic offset fields or fictitious magnetic-field gradients created by an auxiliary light field, we control the state-dependent displacement of the trapping potential or even cancel the fictitious magnetic field, respectively. Based on these techniques, we tune the microwave coupling of motional quantum states. This allows us to establish favorable conditions for microwave sideband cooling which we then use to reduce the mean number of motional quanta along the direction of the displacement to $\langle n \rangle = 0.3(1)$. Finally, we determine the heating rate of the trapped atoms. This shows that the inherent fictitious magnetic field in optical microtraps expands the experimental toolbox for interrogating and manipulating cold atoms.

*schneeweiss@ati.ac.at

†arno.rauschenbeutel@ati.ac.at

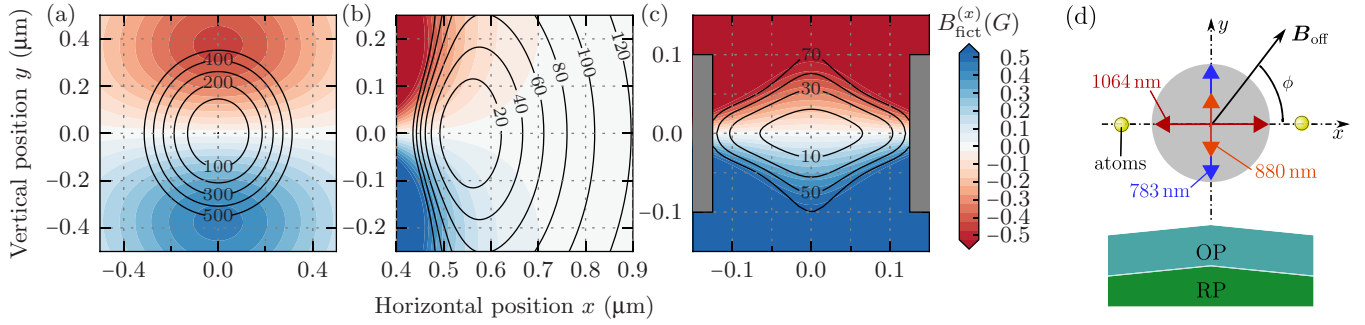


FIG. 1. (a)–(c) Examples of scalar trapping potential and fictitious field for three configurations of microtraps. The plots show transverse cuts through the trap minimum, where contours of the scalar potential are shown as black lines with labels in microkelvin, and the fictitious field is color coded. For the latter, only the dominant x component is shown. In all cases, the propagation direction of the relevant laser is into the plane (along $-z$), and the laser is polarized along y . (a) Laser beam at a wavelength of 850 nm and a power of 5.2 mW, focused down to a waist radius of $0.7 \mu\text{m}$ to trap ^{87}Rb [30]. The trap depth is 1.5 mK. (b) Two-color dipole trap for Cs atoms close to a nanofiber with 250 nm radius whose axis is centered at $x = y = 0$. Trap parameters are given in the main text. (c) Trapping potential for Cs atoms generated by 793-nm-wavelength light propagating in the fundamental mode of a dual SiN nanobeam (gray) with 250 nm gap, 293 nm width, and 200 nm thickness. The parameters resemble those of Ref. [37], but the photonic-crystal structure has not been taken into account. (d) Illustration of the experimental geometry. The orientations of the polarization planes of the nanofiber-guided fields are indicated by double arrows, and respective wavelengths are denoted. For microwave sideband cooling, two external circularly polarized laser fields (OP and RP; see main text) impinge on the atoms from below.

Optical dipole traps rely on the intensity-dependent energy shift of the atomic ground state for an atom exposed to an optical field which is far-detuned with respect to the atomic resonance. For alkali-metal atoms, the interaction Hamiltonian is [33]

$$\hat{V} = -\frac{1}{4}\alpha_s|\mathcal{E}|^2 + i\alpha_v\frac{(\mathcal{E}^* \times \mathcal{E}) \cdot \hat{F}}{8F}. \quad (1)$$

Here, α_s and α_v are, respectively, the scalar and vector polarizabilities, \mathcal{E} is the positive-frequency electric field envelope, and \hat{F} is the total angular momentum operator. The second term of Eq. (1) is equivalent to a magnetic interaction $g_F\mu_B\mathbf{B}_{\text{fict}} \cdot \hat{F}$ with a fictitious magnetic field,

$$\mathbf{B}_{\text{fict}} = \frac{\alpha_v}{8g_F\mu_B F}i(\mathcal{E}^* \times \mathcal{E}), \quad (2)$$

where g_F is the hyperfine Landé factor and μ_B the Bohr magneton. We note that the magnitude of the term $i(\mathcal{E}^* \times \mathcal{E})$ is maximal for a circularly polarized field and zero for linear polarization. For the cases relevant to this work, only the magnitude and sign of \mathbf{B}_{fict} vary in the region around the minimum of the optical potential, but not the overall direction. In the presence of an external offset field \mathbf{B}_{off} , we let \mathbf{B}_{off} define the quantization axis. A spatially varying component of \mathbf{B}_{fict} parallel to \mathbf{B}_{off} hence induces a position-dependent Zeeman shift, through a term proportional to \hat{F}_z in the Hamiltonian, while an orthogonal component can induce spin flips through a term proportional to \hat{F}_x . The effect of the latter, which was used, for instance, to perform degenerate Raman cooling [20,21], is strongly suppressed for a large offset field.

In general, fictitious magnetic fields cannot be neglected for propagating optical modes with a cross section comparable to the wavelength. This is exemplified in Fig. 1 for three experimentally relevant cases of atoms in microtraps. Important insight can be gained for the simple case of a strongly focused Gaussian laser beam. The solution to Maxwell's equations can be written as a series in the diffraction angle

$\theta = \lambda/(\pi w_0)$ [34,35], where w_0 is the waist radius, and λ the wavelength. The zeroth-order term $\mathcal{E}^{(0)}$ is the TEM solution to the paraxial equation with purely transverse polarization. Here, the latter is assumed to be parallel to the unit vector \mathbf{u}_y along y . The first-order correction is a longitudinal component $\mathcal{E}^{(1)} \propto iy\theta\mathcal{E}^{(0)}\mathbf{u}_z$, which oscillates in quadrature to $\mathcal{E}^{(0)}$. The interference of $\mathcal{E}^{(0)}$ and $\mathcal{E}^{(1)}$ thus gives rise to elliptical polarization that lies in the y - z plane. In the focal plane ($z = 0$) and for the TEM₀₀ mode, this elliptical polarization leads to a fictitious magnetic field that is perpendicular to the y - z plane,

$$\mathbf{B}_{\text{fict}}^{(1)} = \frac{\alpha_v}{8g_F\mu_B F}\left(-2\mathbf{u}_x\theta\frac{y}{w_0}|\mathcal{E}_{\text{max}}^{(0)}|^2e^{-2(x^2+y^2)/w_0^2}\right), \quad (3)$$

where $\mathcal{E}_{\text{max}}^{(0)}$ is the value of $\mathcal{E}^{(0)}$ at the origin. Using Eqs. (1)–(3) we calculate the scalar part of the trapping potential and the fictitious magnetic field, both shown in Fig. 1(a). If we approximate the potential at $x = z = 0$ by $ky^2/2 + gy$, where $k = \alpha_s|\mathcal{E}_{\text{max}}^{(0)}|^2/w_0^2$ and $g = g_F\mu_B m_F b_f$ with $b_f = d\mathbf{B}_{\text{fict}}^{(1)}/dy|_{x=z=0}$, we find that the different Zeeman states have their respective potential minimum displaced by $\Delta y = -g/k = \frac{1}{4\pi}\frac{\alpha_v}{\alpha_s}\frac{m_F}{F}\lambda$. This must be compared to the vertical extent of the wave function $\sigma_y = [\hbar^2/(kM)]^{1/4}$, where M is the atomic mass. For the trap parameters used for Fig. 1(a), for example, $|\Delta y| \approx |\frac{m_F}{F}| \times 12 \text{ nm}$ and $\sigma_y \approx 26 \text{ nm}$. Hence, the intrinsic fictitious field has a significant impact on the trapping potential, which will be important for the manipulation of the internal and external states of the atom.

The situation is comparable for atoms trapped in the evanescent fields of dielectric waveguides. Although the specific geometry of the dielectric, and the even tighter field confinement, will give rise to additional components of the fictitious field, also here the dominant component is oriented perpendicular to the y - z plane. For the example of a nanofiber-based trap for Cs [11,36], the scalar potential and fictitious field are shown in Fig. 1(b). We note that the field here is solely due to the blue-detuned trap laser, as the standing wave

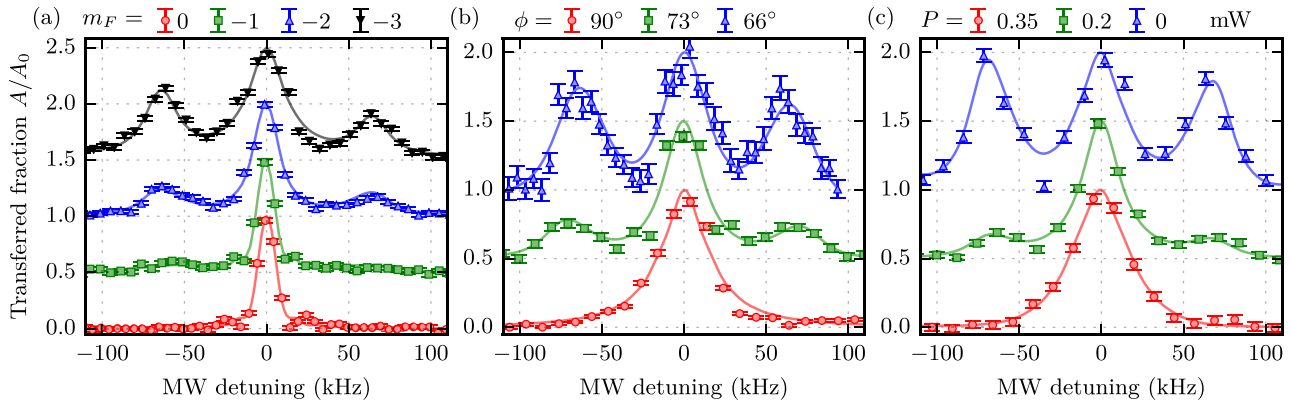


FIG. 2. Microwave (MW) spectra for (a) π transitions between different Zeeman states, (b) different angles of the offset magnetic field, and (c) different powers of the tune-out laser. The ratio A/A_0 indicates the number of transferred atoms, normalized to the amplitude of the carrier. The MW detuning is defined relative to the carrier transition, and different datasets are offset vertically for clarity. In (a) the initial state is $F = 3$, while it is $F = 4$ in (b) and (c). Solid lines are fits to an optical-Bloch-equation model. Error bars stem from the standard error of the nonlinear fits used for the estimation of the number of atoms.

formed by the red-detuned trap laser does not contribute. As a final example, in Fig. 1(c) we show a trap for Cs atoms based on 793-nm-wavelength guided light in a dual SiN nanobeam [37], and we expect a comparable result for slotted nanofibers [38].

In the scope of this work, we experimentally explore the case in Figs. 1(b) and 1(d), i.e., the nanofiber-based two-color dipole trap for cesium atoms [11]. The nanofiber used in our experiment features a waist diameter of 500 nm. The trapping potential is formed by a running-wave field with a free-space wavelength of 783 nm and a power of 17.8 mW, and an orthogonally polarized standing-wave field at 1064 nm wavelength with a power of 1.25 mW per beam, resulting in a trap depth of 163 μ K. By applying a microwave field at a frequency around the hyperfine splitting between the $F = 4$ and $F = 3$ ground state manifolds, one can drive transitions from a state $|F = 4, m_F, n\rangle$ to $|F = 3, m'_F, n'\rangle$. Here, n and n' are the respective quantum numbers for the motional states. The transition strength is given by the effective Rabi frequency $\Omega_{n,n'} = \Omega C_{n,n'}$, where Ω is the bare Rabi frequency and $C_{n,n'}$ is the Franck-Condon factor [25]. For $n \neq n'$, one way to obtain nonzero $C_{n,n'}$ is to introduce a relative displacement of the potentials associated with the initial and final states. This leads to the appearance of sidebands in the microwave spectrum. For our system, the displacement is predominantly along y , and we expect to see sidebands corresponding to the trap frequency ω_y along this direction.

In order to obtain microwave spectra, we load atoms into the nanofiber-based trap in their $F = 4$ hyperfine ground state. We then ramp up an external homogeneous offset field to $B_{\text{off}} = 1.56$ G with an angle $\phi = 66^\circ$ with respect to the x axis. After this, we find the majority of atoms in $m_F = -4$, presumably because of a residual \hat{F}_x magnetic interaction during the ramp of the offset field. The high degree of spin polarization then comes at the expense of an increased number of motional excitations. A microwave pulse with a boxcar-shaped envelope at a given frequency transfers atoms in a specific Zeeman state from $F = 4$ to $F = 3$. The pulse amplitude corresponds to $\Omega \approx 2\pi \times 10$ kHz and its duration maximizes the population transfer on the carrier transition. Atoms remaining in $F = 4$ are removed by applying a free-space push-out laser beam. The

fraction A of transferred atoms is then estimated by optically pumping them back to $F = 4$, and measuring the absorption of a weak nanofiber-guided light field on the cycling transition of the D_2 line. This fraction is normalized to the initial atom number, measured by the same means at the beginning of each experimental sequence.

The displacement Δy of the trapping potentials depends on the Zeeman state and the gradient of the effective magnetic field. Figure 2 shows a collection of microwave spectra that confirm these dependencies. Microwave spectra for π transitions addressing different m_F states are shown in Fig. 2(a). As an exception, here, the atoms are prepared in $F = 3$ before taking the spectra. For $m_F = 0$, we observe only a carrier transition. For $m_F \neq 0$, sidebands appear and become more pronounced for increasing $|m_F|$. The positions of the sidebands agree reasonably well with our calculated value $\omega_y = 2\pi \times 77$ kHz, and we observe no sidebands at the two other trap frequencies $(\omega_x, \omega_z) = 2\pi \times (128, 198)$ kHz.

Figures 2(b) and 2(c) show two means to tune the strength of the sidebands for a given transition. For a sufficiently large offset field, Δy is proportional to the derivative of the the projection of \mathbf{B}_{fict} onto \mathbf{B}_{off} . An offset field at an angle ϕ hence reduces the displacement by a factor $\cos \phi$. This is demonstrated in Fig. 2(b), which shows the transition from large to vanishing sideband amplitude when ϕ is varied between 66° and 90° . For every setting of ϕ , we slightly adjusted the polarizations of the trap laser fields in order to minimize the width of the microwave transitions. Another possibility to tune the displacement is by changing \mathbf{B}_{fict} itself, using an additional nanofiber-guided laser field operating at the tune-out wavelength of about 880 nm [39]. At this wavelength, the scalar polarizability vanishes, and the scalar potential is not affected. The vector polarizability has the opposite sign than for light at 783 nm, such that the total fictitious field is reduced when the two fields are copropagating and identically polarized. One can clearly see from Fig. 2(c) the dependence of the sideband height on the applied tune-out laser power. For 0.35 mW, the fictitious field at the position of the atoms is almost completely compensated, which fits very well with the theoretical expectation of about 0.36 mW.

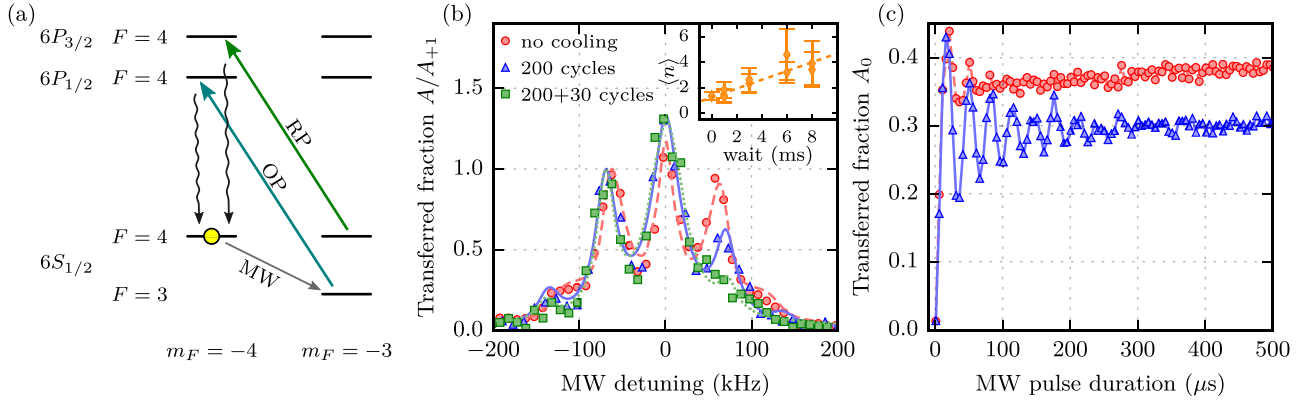


FIG. 3. Microwave sideband cooling scheme and results. (a) Diagram of our cooling scheme with relevant levels and transitions for cesium. One cooling cycle consists of a microwave (MW) pulse and optical pumping (OP, RP) followed by spontaneous emission. (b) Experimental microwave spectra on the $|F = 4, m_F = -4\rangle \rightarrow |F = 3, m_F = -3\rangle$ transition without cooling (red circles), after the application of 200 cooling cycles (blue triangles), and for 30 additional cycles without RP (green squares). The spectra are recentered to compensate for a temperature-dependent shift of the transition frequency, on the order of 20 kHz, that can be attributed to an x -dependent differential light shift induced by the trapping lasers. Spectra are normalized to the first left sideband. Lines are fit results (see text). The inset in (b) shows the evolution of the mean number of motional excitations for a variable waiting time following the cooling sequence. A linear fit (dashed line) gives a heating rate of 0.34(1) quanta/ms. (c) Rabi oscillations on the carrier of the $|F = 4, m_F = -4\rangle \rightarrow |F = 3, m_F = -3\rangle$ transition without cooling (red circles) and after 200 cooling cycles (blue triangles). The transferred fraction A_0 is normalized to the initial atom number. The difference in the steady-state transfer probabilities reflects atom losses that can be attributed to both a finite lifetime in our trap and losses to other m_F states during the cooling sequence. Error bars in (b) and (c) are smaller than the symbol size.

The temperature of the atomic ensemble can be estimated via the ratio of the amplitude of the sidebands. Assuming an ideal harmonic oscillator, the mean number of motional excitations is given by $\langle n \rangle = A_{-1}/(A_{+1} - A_{-1})$, where A_m is the amplitude of the sideband for the transition $n \rightarrow n + m$. In our case, the relevant sidebands have almost equal amplitude, meaning that $\langle n \rangle \gg 1$. However, the fact that we can resolve the sidebands in the microwave spectra enables us to implement cooling. With the atoms initially in $|F = 4, m_F = -4\rangle$, a single cooling cycle, sketched in Fig. 3(a), consists of a 20- μ s-long microwave pulse on the $n \rightarrow n - 1$ sideband with bare Rabi frequency around $2\pi \times 40$ kHz. The atoms are then optically pumped back to the initial state using a σ^- -polarized light field on the Cs D_1 line, labeled OP [see Fig. 1(d)]. During the optical pumping, the atoms are brought back to the initial state, but also have a finite probability to spontaneously decay into $|F = 4, m_F = -3\rangle$. Those atoms are re-integrated into the cooling cycle with a σ^- -polarized repumping field, labeled RP, on the Cs D_2 transition. Both OP and RP are on for 10 μ s, and we leave OP on for another 10 μ s to pump all atoms out of $F = 3$.

Figure 3(b) shows microwave spectra without cooling and after 200 cooling cycles. As expected, the cooling results in a relative reduction of A_{-1} . To obtain quantitative information about the cooling efficiency, we fit the experimental data using an optical Bloch equation model. The model assumes a one-dimensional potential and a thermal distribution of motional excitations. It takes into account the calculated anharmonicity of the trap and a finite dephasing time for the microwave transitions. Free parameters for the fit are the mean excitation number $\langle n \rangle$, trap frequency ω_y , bare Rabi frequency Ω , displacement $\delta = \Delta y' - \Delta y$ between the initial and final potentials, a finite dephasing time T_2 , as well as an overall amplitude and a horizontal offset. As can be

seen in Fig. 3(b), the fit reproduces well the shape of the spectra. The obtained values for ω_y , Ω , and T_2 agree well with expectations. For the data with preceding cooling, we get $\delta/\sigma_y = 0.56(6)$, in perfect agreement with the calculated value of 0.56. Without cooling, the fit gives $\delta/\sigma_y = 0.34(2)$. We attribute this discrepancy to the fact that hotter atoms are on average further away from the fiber [11], where the scaling of the effective scalar potential and fictitious field along y leads to a reduced displacement. Finally, the fit allows us to extract a mean excitation number of $\langle n \rangle = 10(2)$ without, and $\langle n \rangle = 1.4(3)$ with cooling, corresponding to a temperature around 6 μ K.

We identify four main mechanisms likely to limit the final temperature: background heating, imperfect polarization of the RP beam, projection heating from the OP beam [26], and off-resonant microwave excitation of the carrier transition during the cooling cycle. We measured the background heating rate in our system by introducing a variable waiting time after the last cooling cycle [see inset of Fig. 3(b)]. We extract a heating rate of 0.34(1) quanta/ms from a linear fit, corresponding to 0.014 quanta per cooling cycle. This heating rate should not be a significant limitation for the measured mean excitation number of $\langle n \rangle = 1.4(3)$. Another candidate is imperfect dark-state purity: The OP and RP beams are mutually parallel and, for technical reasons, propagate at an angle of around 30° to the offset magnetic field, which limits the polarization purity. As a consequence, the state $|F = 4, m_F = 4\rangle$ is not the desired dark state of the cooling sequence, and additional photon scattering leads to spurious heating. We experimentally investigated this effect by adding 30 cooling cycles during which the RP light is off [see green data points and associated fit in Fig. 3(b)]. We then obtain a mean excitation number of $\langle n \rangle = 0.3(1)$, at the expense of losing a third of the atoms. These atoms most probably decayed to other m_F states during the optical

pumping phase. In the absence of the RP light, they are then excluded from the cooling cycle and are no longer detected in our spectra. Finally, we estimate that projection heating contributes 0.16 quanta per cooling cycle, and that atoms that are in the motional ground state still exhibit a 20% probability of undergoing an off-resonant microwave transition.

As another indication of successful cooling, we record Rabi oscillations between the states $|F=3, m_F=-3\rangle$ and $|F=4, m_F=-4\rangle$ by applying a microwave pulse of variable duration on the carrier transition without cooling and after 200 cooling cycles. Figure 3(c) shows the transferred population as a function of pulse duration. Without cooling, the visibility of the Rabi oscillations decreases rapidly because all the motional states involved have different effective Rabi frequencies. After cooling, the mean excitation number is lowered and only few motional states contribute. As a consequence, the dephasing time is increased by an order of magnitude.

In summary, we investigated the strongly inhomogeneous fictitious magnetic fields that arise from the tight confinement of light fields used to create optical microtraps. Taking advantage of these fictitious fields, we demonstrated techniques that allow one to probe and to manipulate cold atoms. Using microwave spectroscopy, we showed for the specific case of nanofiber-trapped cesium atoms that the resulting state-dependent potentials can be tailored with external magnetic fields or with additional fiber-guided light. We exploited the state-dependent potentials to probe important parameters of the trap and the atoms therein. By performing microwave

sideband cooling, we reached temperatures close to the ground state for the motion of the atoms in the azimuthal direction. State-dependent potentials in the radial or the longitudinal directions, respectively, can in principle be obtained by tilting the polarization plane of the tune-out laser, or changing the standing wave of the laser at 1064 nm wavelength to a lin- θ -lin configuration [36]. This should enable a generalization of the cooling technique to three dimensions. Besides its general relevance for experiments with atoms in optical microtraps, the cooling technique may, in particular, facilitate studies of self-organization [40,41] and lateral light forces [42–45] for atoms close to waveguides. In addition, it may provide a well-defined starting point for loading atoms into surface-induced potentials [46] or for the investigation of collapse and revival dynamics in nanofiber-based traps [47]. Furthermore, our work gives an example of the utility of the inherent fictitious magnetic fields in optical microtraps, which may be advantageous for addressing and manipulating atoms near photonic nanostructures.

We thank Igor Mazets for helpful discussions, and Clément Sayrin for valuable insights, discussions, and feedback during the preparation of the experiment. Financial support by the Austrian Science Fund (FWF, SFB NextLite Project No. F 4908-N23, and DK CoQuS Project No. W 1210-N16) and the European Research Council (Consolidator Grant NanoQuaNt) is gratefully acknowledged. C.C. acknowledges support by the European Commission (Marie Curie IF Grant No. 658556).

-
- [1] D. M. Stamper-Kurn, M. R. Andrews, A. P. Chikkatur, S. Inouye, H.-J. Miesner, J. Stenger, and W. Ketterle, *Phys. Rev. Lett.* **80**, 2027 (1998).
- [2] S. R. Granade, M. E. Gehm, K. M. O'Hara, and J. E. Thomas, *Phys. Rev. Lett.* **88**, 120405 (2002).
- [3] I. Bloch, *Nat. Phys.* **1**, 23 (2005).
- [4] Y. O. Dudin, L. Li, and A. Kuzmich, *Phys. Rev. A* **87**, 031801 (2013).
- [5] H. Katori, M. Takamoto, V. G. Pal'chikov, and V. D. Ovsiannikov, *Phys. Rev. Lett.* **91**, 173005 (2003).
- [6] N. Schlosser, G. Reymond, I. Protchenko, and P. Grangier, *Nature (London)* **411**, 1024 (2001).
- [7] Y. R. P. Sortais, H. Marion, C. Tuchendler, A. M. Lance, M. Lamare, P. Fournet, C. Armellin, R. Mercier, G. Messin, A. Browaeys, and P. Grangier, *Phys. Rev. A* **75**, 013406 (2007).
- [8] T. Wilk, A. Gaëtan, C. Evellin, J. Wolters, Y. Miroshnychenko, P. Grangier, and A. Browaeys, *Phys. Rev. Lett.* **104**, 010502 (2010).
- [9] X. L. Zhang, L. Isenhower, A. T. Gill, T. G. Walker, and M. Saffman, *Phys. Rev. A* **82**, 030306 (2010).
- [10] A. M. Kaufman, B. J. Lester, M. Foss-Feig, M. L. Wall, A. M. Rey, and C. A. Regal, *Nature (London)* **527**, 208 (2015).
- [11] E. Vetsch, D. Reitz, G. Sagué, R. Schmidt, S. T. Dawkins, and A. Rauschenbeutel, *Phys. Rev. Lett.* **104**, 203603 (2010).
- [12] A. Goban, K. S. Choi, D. J. Alton, D. Ding, C. Lacroûte, M. Pototschnig, T. Thiele, N. P. Stern, and H. J. Kimble, *Phys. Rev. Lett.* **109**, 033603 (2012).
- [13] A. Goban, C.-L. Hung, S.-P. Yu, J. Hood, J. Muniz, J. Lee, M. Martin, A. McClung, K. Choi, D. Chang, O. Painter, and H. Kimble, *Nat. Commun.* **5**, 3808 (2014).
- [14] D. E. Chang, V. Vuletić, and M. D. Lukin, *Nat. Photonics* **8**, 685 (2014).
- [15] J. S. Douglas, H. Habibian, C.-L. Hung, A. V. Gorshkov, H. J. Kimble, and D. E. Chang, *Nat. Photonics* **9**, 326 (2015).
- [16] C. Cohen-Tannoudji and J. Dupont-Roc, *Phys. Rev. A* **5**, 968 (1972).
- [17] J. Dalibard and C. Cohen-Tannoudji, *J. Opt. Soc. Am. B* **6**, 2023 (1989).
- [18] C. Y. Park, J. Y. Kim, J. M. Song, and D. Cho, *Phys. Rev. A* **65**, 033410 (2002).
- [19] H. Perrin, A. Kuhn, I. Bouchoule, and C. Salomon, *Europhys. Lett.* **42**, 395 (1998).
- [20] S. E. Hamann, D. L. Haycock, G. Klose, P. H. Pax, I. H. Deutsch, and P. S. Jessen, *Phys. Rev. Lett.* **80**, 4149 (1998).
- [21] A. J. Kerman, V. Vuletić, C. Chin, and S. Chu, *Phys. Rev. Lett.* **84**, 439 (2000).
- [22] O. Mandel, M. Greiner, A. Widera, T. Rom, T. W. Hänsch, and I. Bloch, *Phys. Rev. Lett.* **91**, 010407 (2003).
- [23] M. Karski, L. Förster, J. Choi, A. Steffen, W. Alt, D. Meschede, and A. Widera, *Science* **325**, 174 (2009).
- [24] N. Lundblad, J. M. Obrecht, I. B. Spielman, and J. V. Porto, *Nat. Phys.* **5**, 575 (2009).
- [25] L. Förster, M. Karski, J. M. Choi, A. Steffen, W. Alt, D. Meschede, A. Widera, E. Montano, J. H. Lee, W. Rakreungdet, and P. S. Jessen, *Phys. Rev. Lett.* **103**, 233001 (2009).

- [26] X. Li, T. A. Corcovilos, Y. Wang, and D. S. Weiss, *Phys. Rev. Lett.* **108**, 103001 (2012).
- [27] B. Richards and E. Wolf, *Proc. R. Soc. London, Ser. A* **253**, 358 (1959).
- [28] K. Y. Bliokh and F. Nori, *Phys. Rep.* **592**, 1 (2015).
- [29] P. Lodahl, S. Mahmoodian, S. Stobbe, P. Schneeweiss, J. Volz, A. Rauschenbeutel, H. Pichler, and P. Zoller, [arXiv:1608.00446](https://arxiv.org/abs/1608.00446).
- [30] A. M. Kaufman, B. J. Lester, and C. A. Regal, *Phys. Rev. X* **2**, 041014 (2012).
- [31] C. Lacroûte, K. S. Choi, A. Goban, D. J. Alton, D. Ding, N. P. Stern, and H. J. Kimble, *New J. Phys.* **14**, 023056 (2012).
- [32] J. D. Thompson, T. G. Tiecke, A. S. Zibrov, V. Vuletić, and M. D. Lukin, *Phys. Rev. Lett.* **110**, 133001 (2013).
- [33] Fam Le Kien, P. Schneeweiss, and A. Rauschenbeutel, *Eur. Phys. J. D* **67**, 92 (2013).
- [34] M. Lax, W. H. Louisell, and W. B. McKnight, *Phys. Rev. A* **11**, 1365 (1975).
- [35] Y. Salamin, *Appl. Phys. B* **86**, 319 (2007).
- [36] Fam Le Kien, P. Schneeweiss, and A. Rauschenbeutel, *Phys. Rev. A* **88**, 033840 (2013).
- [37] C.-L. Hung, S. M. Meenehan, D. E. Chang, O. Painter, and H. J. Kimble, *New J. Phys.* **15**, 083026 (2013).
- [38] M. Daly, V. G. Truong, and S. Nic Chormaic, *Opt. Express* **24**, 14470 (2016).
- [39] B. Arora, M. S. Safronova, and C. W. Clark, *Phys. Rev. A* **84**, 043401 (2011).
- [40] D. E. Chang, J. I. Cirac, and H. J. Kimble, *Phys. Rev. Lett.* **110**, 113606 (2013).
- [41] T. Griebner and H. Ritsch, *Phys. Rev. Lett.* **111**, 055702 (2013).
- [42] S. Scheel, S. Y. Buhmann, C. Clausen, and P. Schneeweiss, *Phys. Rev. A* **92**, 043819 (2015).
- [43] F. J. Rodriguez-Fortuno, N. Engheta, A. Martinez, and A. V. Zayats, *Nat. Commun.* **6**, 8799 (2015).
- [44] S. Sukhov, V. Kajorndejnukul, R. R. Naraghi, and A. Dogariu, *Nat. Photonics* **9**, 809 (2015).
- [45] F. Kalhor, T. Thundat, and Z. Jacob, *Appl. Phys. Lett.* **108**, 061102 (2016).
- [46] D. E. Chang, K. Sinha, J. M. Taylor, and H. J. Kimble, *Nat. Commun.* **5**, 4343 (2014).
- [47] Fam Le Kien, K. Hakuta, D. Reitz, P. Schneeweiss, and A. Rauschenbeutel, *Phys. Rev. A* **87**, 063607 (2013).